Electronic Supplementary Material (ESI) for ChemComm.

A calixarene-based fluorescent ratiometric temperature probe

Brunella Bardi, Irene Tosi, Federica Faroldi, Laura Baldini, Francesco Sansone, Cristina Sissa and Francesca Terenziani

Dipartimento di Scienze Chimiche, della Vita e della Sostenibilità Ambientale, Università di Parma, Parco Area delle Scienze 17/A, 43124 Parma, Italy

SUPPORTING INFORMATION

Table of contents

1. GENERAL METHODS

All moisture sensitive reactions were carried out under Nitrogen or Argon atmosphere, using previously oven-dried glassware. Dry solvents were prepared according to standard procedures, distilled before use and stored over 3 or 4 Å molecular sieves. Most of the solvents and reagents were obtained from commercial sources and used without further purification. Analytical TLC were performed using prepared plates of silica gel (Merck 60 F-254 on aluminum) and then revealed with UV light. Merck silica gel 60 (70-230 mesh) was used for flash chromatography and for preparative TLC plates. ^{1}H NMR and ^{13}C spectra were recorded on Bruker AV300 and Bruker AV400 spectrometers (observation of ^{1}H nucleus at 300 MHz and 400 MHz respectively, and of ^{13}C nucleus at 75 MHz and 100 MHz respectively). All chemical shifts are reported in part per million (ppm) using the residual peak of the deuterated solvent, whose values are referred to tetramethylsilane (TMS, δ_{TMS} = 0), as internal standard. All ^{13}C NMR spectra were performed with proton decoupling. High resolution mass spectra were recorded on a LTQ Orbitrap XL instrument in positive mode using acetonitrile or methanol as solvents. Melting points were determined on an Electrothermal apparatus in closed capillaries.

Spectra grade or HPLC solvents were used to prepare the samples for optical spectroscopy. UV-vis absorption spectra at room temperature for solutions at known concentration were collected with a Perkin-Elmer Lambda650 spectrophotometer. For the evaluation of the molar extinction coefficient, absorbance was measured on solutions of different concentrations and the Lamber-Beer law was verified.
UV-vis absorption spectra at variable temperature were measured with an Oxford Instruments OptistatDN cryostat adapted into an Edinburgh FLS1000 spectrofluorometer equipped with an accessory for the detection of the transmitted light.
Emission spectra were collected with a Horiba-Jobin Ivon Fluoromax 3 fluorometer. Fluorescence quantum yields were measured on diluted solutions (absorbance < 0.1), to minimize inner-filter effects. Fluoresceine in NaOH 0.1 M (ϕ = 0.9) was used as the fluorescence standard.

5,17-dihydroxycarbonyl-25,26,27,28-tetrapropoxycalix[4]arene (**4**),[1] 5-hydroxycarbonyl-25,26,27,28-tetrapropoxycalix[4]arene (**5**)[2] and N-(7-Nitrobenz-2-oxa-1,3-diazol-4-yl)ethylendiamine (**NBD-NH$_2$**)[3] were synthesized according to literature procedures.

2. SYNTHESIS

Comumarin 343 ethylendiamine derivative (**Coum-NH$_2$**) was synthesized according to a modification of a literature procedure (0 S1).[4]

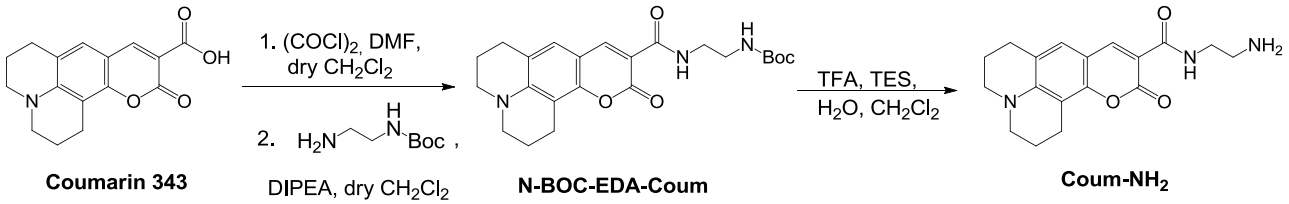

Scheme S1. Synthesis of **Coum-NH$_2$**.

N-Boc-EDA-Coum

To a stirring solution of Coumarin343 (100 mg, 0.35 mmol) in dry CH_2Cl_2 (18 mL), $(COCl)_2$ (460 µL, 5.26 mmol, WARNING: oxalyl chloride causes severe skin burns and eye damage, is toxic if inhaled, may cause respiratory irritation) and dry DMF (10 µL), were slowly added and the color of the solution became immediately red. The reaction mixture was stirred for 3 h at rt, then it was concentrated under reduced pressure obtaining a

red solid (the acyl chloride of Coumarin343), which was redissolved in dry CH_2Cl_2 (10 mL). To this solution, a solution of N-*tert*-butoxycarbamoilethylendiamine (191 mg, 1.23 mmol) and DIPEA (54 µL, 3.08 mmol) in dry CH_2Cl_2 (5 mL) was added dropwise. The resulting red mixture was stirred at rt for 48 h, then the reaction was monitored by TLC (CH_2Cl_2-CH_3OH 98:2, v/v) and quenched with H_2O (15 mL). The organic layer was washed with 1N NaOH (1x10 mL) and then with H_2O till neutral pH, dried over Na_2SO_4 and concentrated under reduced pressure obtaining a purple solid. Pure **N-Boc-EDA-Coum** was isolated as a yellow powder by flash column chromatography (CH_2Cl_2/CH_3OH 98:2, v/v) in 56% yield (84 mg, 0.19 mmol).
The product showed the same spectroscopic properties previously reported.[4]

Coum-NH_2

N-Boc-EDA-Coum (84 mg, 0.19 mmol) was dissolved in a mixture of CH_2Cl_2/TFA/TES/H_2O (47.5:47.5:2.5:2.5, v/v/v/v, 5 mL), the reaction was allowed to proceed at rt and was monitored by TLC (CH_2Cl_2-CH_3OH 98:2, v/v). After 2 h the reaction mixture was concentrated under reduced pressure, the brown crude was dissolved in CH_2Cl_2 and concentrated again (3 times), then it was redissolved in CH_2Cl_2 (15 mL) and washed with 5% aqueous $NaHCO_3$ (15 mL) and H_2O (15 mL). Pure **Coum-NH_2** was isolated as an orange powder in quantitative yield (60 mg, 0.19 mmol) by evaporating the solvent under vacuum.
The product showed the same spectroscopic properties previously reported.[4]

Compound **1** was synthesized by the reaction of 5,17-dihydroxycarbonyl-25,26,27,28-tetrapropoxycalix[4]arene (**4**),[1] activated as acyl chloride, with an equimolar mixture of **Coum-NH_2** and **NBD-NH_2** (Scheme S2).

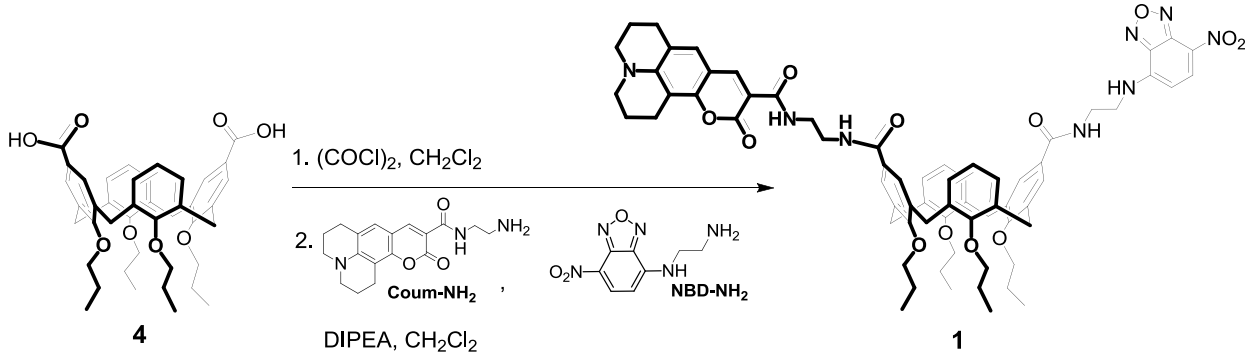

Scheme S2. Synthesis of compound **1.**

Compound 1

$(COCl)_2$ (450 µL, 5.11 mmol, WARNING: oxalyl chloride causes severe skin burns and eye damage, is toxic if inhaled, may cause respiratory irritation) and dry DMF (20 µL) were added to a solution of **4** (120 mg, 0.17 mmol) in dry CH_2Cl_2 (18 mL), and the mixture was stirred at rt for 3 h. After removing the solvent under reduced pressure, the acyl chloride thus obtained was dried for 5 h under vacuum (0.1-0.5 mm Hg). Without further purification, it was redissolved, in dry CH_2Cl_2 (15 mL) and added to a stirred solution of **Coum-NH_2** (64 mg, 0.19 mmol), **NBD-NH_2** (49 mg, 0.19 mmol) and DIPEA (150 µL, 0.85 mmol) in dry CH_2Cl_2 (15 mL). Then, to this brown solution, DIPEA (75 µL, 0.43 mmol) was added. The reaction proceeded at rt for 19 h and was monitored by TLC (CH_2Cl_2/CH_3OH 98/2). The reaction was quenched with H_2O; the organic layer was washed with H_2O (2x50 mL) and dried over anhydrous Na_2SO_4 and concentrated under reduced pressure. The red crude was purified by flash column chromatography (gradient CH_2Cl_2/Acetone 90/10, Acetone) to afford **1** as a dark orange-red powder in 24% yield (50 mg, 0.04 mmol).

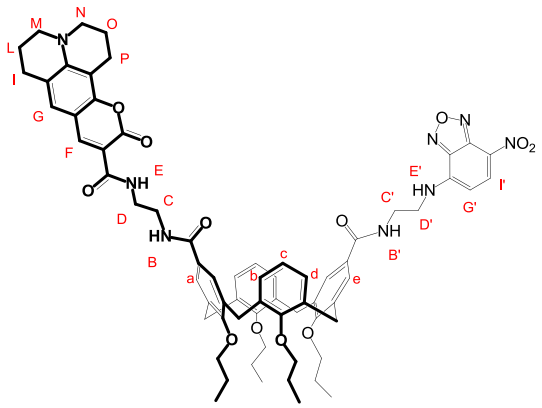

1

M.p.: decomposition over 196°C. ^{1}H NMR (400 MHz, $CDCl_3$) δ (ppm): 9.14 (bs, 1H, H_E); 8.72 (s, 1H, $H_{E'}$); 8.55 (s, 1H, H_F); 8.42 (d, J = 7.2 Hz, 1H, $H_{I'}$); 6.94-6.89 (m, 6H, H_b, H_d, H_B, H_G); 6.70 (s, 2H, H_e), 6.57 (t, J = 7.2 Hz, 2H, H_c); 6.53 (s, 2H, H_a); 6.42 (bs, 1H, $H_{B'}$); 6.13 (d, J = 7.2 Hz, 1H, $H_{G'}$); 4.45 (d, J = 13.6 Hz, 2H, ArC*H*HAr); 4.40 (d, J = 13.2 Hz, 2H, ArC*H*HAr); 3.99 (t, 4H, J = 7.6 Hz, $OCH_2CH_2CH_3$); 3.73-3.63 (m, 8H, $OCH_2CH_2CH_3$, $H_{C'}$ and $H_{D'}$); 3.51 (bs, 2H, H_D); 3.46 (bs, 2H, H_C); 3.34 (t, J = 5.2 Hz, 4H, H_M, H_N); 3.20 (d, J = 13.2 Hz, 2H, ArCH*H*Ar); 3.11 (d, J = 13.6 Hz, 2H, ArCH*H*Ar); 2.85 (t, J = 6.0 Hz, 2H, H_P); 2.72 (t, J = 6.0 Hz, 2H, H_I); 1.98-1.83 (m, 12H, H_O, H_L, $OCH_2CH_2CH_3$); 1.09 (t, J = 7.2 Hz, 3H, $OCH_2CH_2CH_3$); 1.04 (t, J = 7.6 Hz, 3H, $OCH_2CH_2CH_3$); 0.89 (t, J = 7.6 Hz, 6H, $OCH_2CH_2CH_3$). ^{1}H NMR (300 MHz, DMSO-d_6) δ (ppm): 9.56 (bs, 1H, H_E); 8.83 (t, J = 5.5 Hz, 1H, $H_{E'}$); 8.55-8.51 (m, 3H, $H_{I'}$, H_F and H_B); 7.59 (s, 2H, H_e); 7.57 (s, 2H, H_a); 7.20 (s, 1H, H_G); 6.54 (d, J = 9.0 Hz, 1H, $H_{G'}$); 6.25-6.13 (m, 6H, H_b, H_d and H_c); 4.36 (d, J = 13.2 Hz, 2H, ArC*H*HAr); 4.02 (t, 4H, J = 7.8 Hz, $OCH_2CH_2CH_3$); 3.66-3.57 (m, 4H, $OCH_2CH_2CH_3$); 3.55-3.41 (m, 8H, H_C, H_D, $H_{C'}$ and $H_{D'}$); 3.35-3.29 (m, 4H, H_M and H_N); 3.21 (d, J = 13.2 Hz, 2H, ArCH*H*Ar); 3.19 (d, J = 13.2 Hz, 2H, ArCH*H*Ar); 2.73-2.66 (m, 4H, H_P and H_I); 1.96-1.78 (m, 12H, H_O, H_L and $OCH_2CH_2CH_3$); 1.07 (t, J = 7.4 Hz, 6H, $OCH_2CH_2CH_3$); 0.89 (t, J = 7.4 Hz, 6H, $OCH_2CH_2CH_3$). ^{13}C NMR (100 MHz, $CDCl_3$): δ (ppm): 170.1; 168.3; 165.1; 162.8; 158.5; 158.1; 157.3; 152.5; 148.4; 147.6; 144.0; 144.3; 136.5; 136.0; 134.1; 133.9; 129.0; 128.0; 126.9; 126.6; 126.5; 122.9; 122.2; 119.8; 108.3; 107.8; 105.7; 97.9; 77.2; 76.6; 50.2; 49.9; 45.0; 41.4; 39.7; 37.9; 31.0; 29.7; 27.4; 23.4; 23.0; 22.7; 21.0; 20.1; 10.7; 9.8. HR-MS: m/z calculated for $C_{68}H_{74}N_8O_{12}$+H^+ 1217.5324, found 1217.5491 (100%).

Compound **2** was synthesized similarly to compound **1** starting from tetrapropoxycalix[4]arene **5** (Scheme S3).[2]

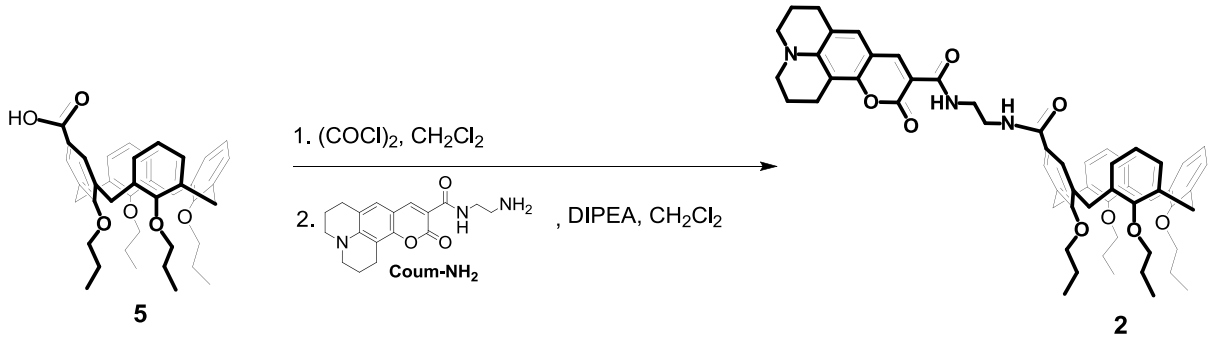

Scheme S3. Synthesis of reference compound **2**.

Compound 2

$(COCl)_2$ (190 µL, 2.18 mmol, WARNING: oxalyl chloride causes severe skin burns and eye damage, is toxic if inhaled, may cause respiratory irritation) and dry DMF (30 µL) were added to a solution of 5-hydroxycarbonyl-25,26,27,28-tetrapropoxycalix[4]arene **5** (68 mg, 0.11 mmol) in dry CH_2Cl_2 (7 mL) and the mixture was stirred

at rt for 4 h. The solvent was removed under vacuum and the resulting acyl chloride was dryed for 2 h under vacuum (0.1-0.5 mm Hg), then redissolved in dry CH_2Cl_2 (15 mL) and added to a solution of **Coum-NH$_2$** (43 mg, 0.13 mmol) and DIPEA (100 µL, 0.65 mmol) in dry CH_2Cl_2 (10 mL). The reaction mixture was stirred at rt for 20 h, then the reaction was quenched by adding H_2O (20 mL). The aqueous layer was extracted with CH_2Cl_2 (4x20 mL) and the combined organic layers were dried over Na_2SO_4 and concentrated under vacuum. The pure product was isolated as a yellow solid by preparative TLC plates (1x CH_2Cl_2-Acetone 80:20, v/v, 1x THF-Cyclohexane 50:50, v/v, 3x CH_2Cl_2-CH_3CN 80:20, v/v) in 25% yield (25 mg, 0.03 mmol).

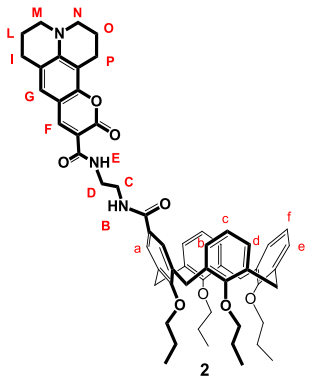

2

M.p: 110 °C. UV-vis: λ_{max} ($CHCl_3$): 438 nm. ^{1}H-NMR (Acetone-d_6, 300MHz): δ (ppm) 9.01 (bs, 1H, NH_E); 8.56 (s, 1H, H_F); 7.73 (bs, 1H, NH_B); 7.41 (s, 2H, H_a); 7.09 (s, 1H, H_G); 6.79 (d, J = 7.4 Hz, 2H, H_e); 6.65 (t, J = 7.0 Hz, 1H, H_f); 6.45-6.32 (m, 6H, Ar H_c, H_b, H_d); 4.49 (d, J = 13.3 Hz, 2H, ArC*H*HAr); 4.47 (d, J = 13.5 Hz, 2H, ArC*H*HAr); 4.02-3.91 (m, 4H, OC*H*$_2$CH$_2$CH$_3$); 3.79 (t, J = 7.1 Hz, 4H, OC*H*$_2$CH$_2$CH$_3$); 3.67-3.62 (m, 2H, H_D); 3.56-3.51 (m, 2H, H_C); 3.41-3.36 (m, 4H, H_N, H_M); 3.21 (d, J = 13.5 Hz, 2H, eq ArCH*H*Ar); 3.15 (d, J = 13.3 Hz, 2H, eq ArCH*H*Ar); 2.85-2.71 (m, 4H, H_I, H_P); 2.00-1.90 (m, 12H, OCH$_2$C*H*$_2$CH$_3$, H_L, H_O); 1.06 (t, J = 7.5 Hz, 6H, OCH$_2$CH$_2$C*H*$_3$); 0.98 (t, J = 7.5 Hz, 6H, OCH$_2$CH$_2$C*H*$_3$). ^{13}C-NMR (Acetone-d_6, 75MHz): δ (ppm) 167.6; 164.9; 163.1; 160.6; 157.9; 156.9; 153.7; 149.2; 148.6; 136.7; 136.6; 135.3; 134.7; 134.4; 129.6; 129.4; 128.9; 128.8; 128.6; 128.1; 120.7; 109.6; 106.2; 77.7; 77.5; 77.4; 69.4; 50.8; 50.4; 41.6; 39.7; 30.7; 23.4; 21.9; 20.9; 10.9; 10.6. HR-MS: m/z calcd for $C_{59}H_{67}N_3O_8$+H^+ 946.4989, found 946.5016 (100%), m/z calcd for $C_{59}H_{67}N_3O_8$+Na^+ 968.4809, found 968.4833 (50%).

3. NMR SPECTRA OF PRODUCTS

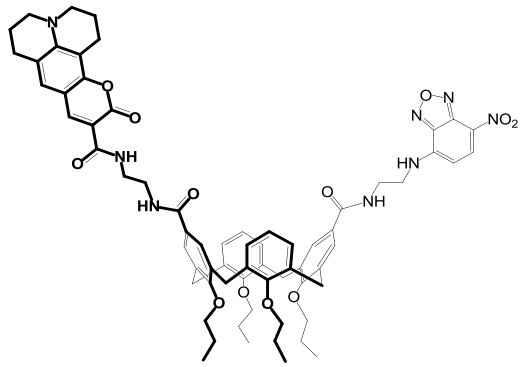

1

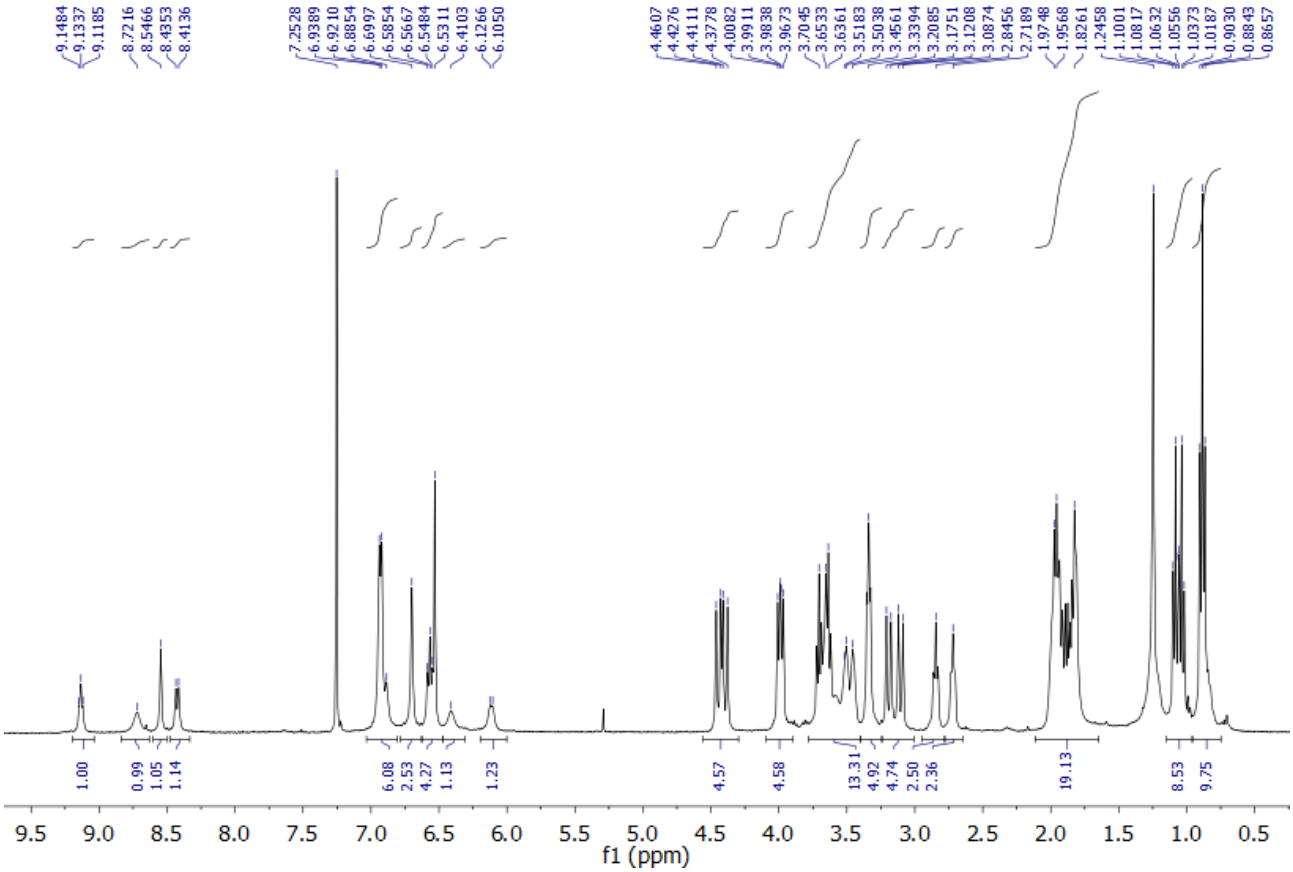

^{1}H NMR spectrum ($CDCl_3$, 400 MHz) of compound **1**

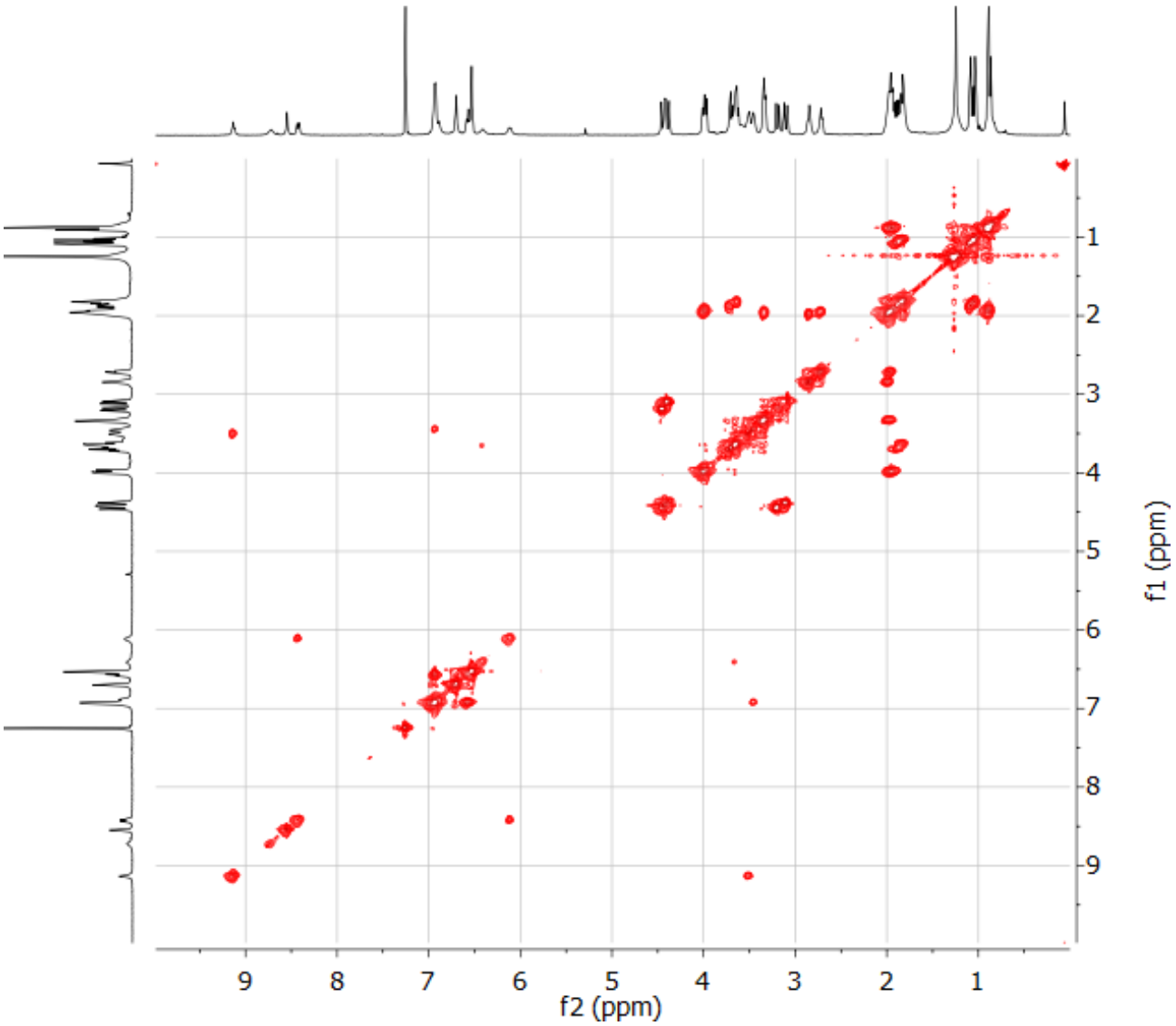

COSY ^{1}H NMR spectrum ($CDCl_3$, 400 MHz) of compound **1**

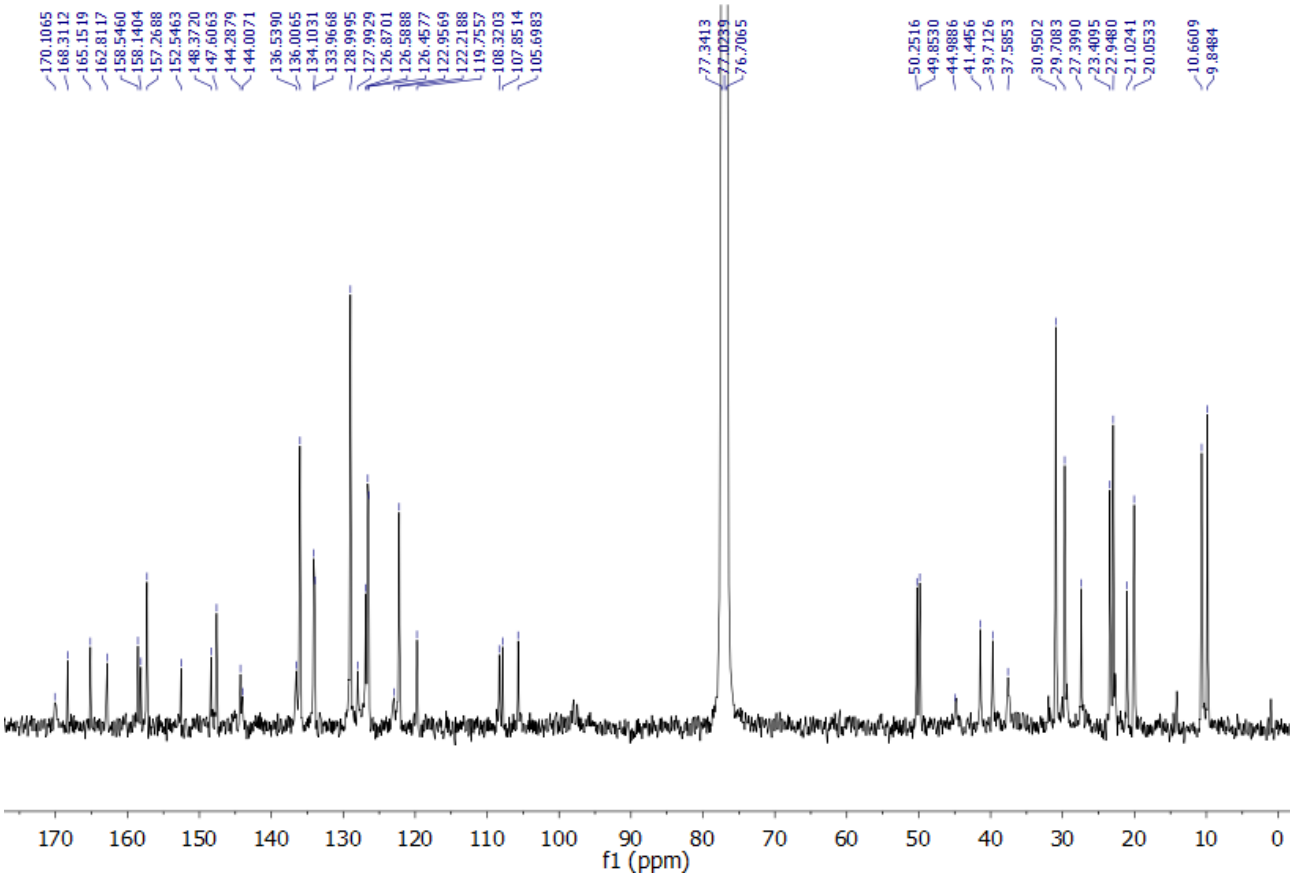

^{13}C NMR spectrum ($CDCl_3$, 100 MHz) of compound **1**

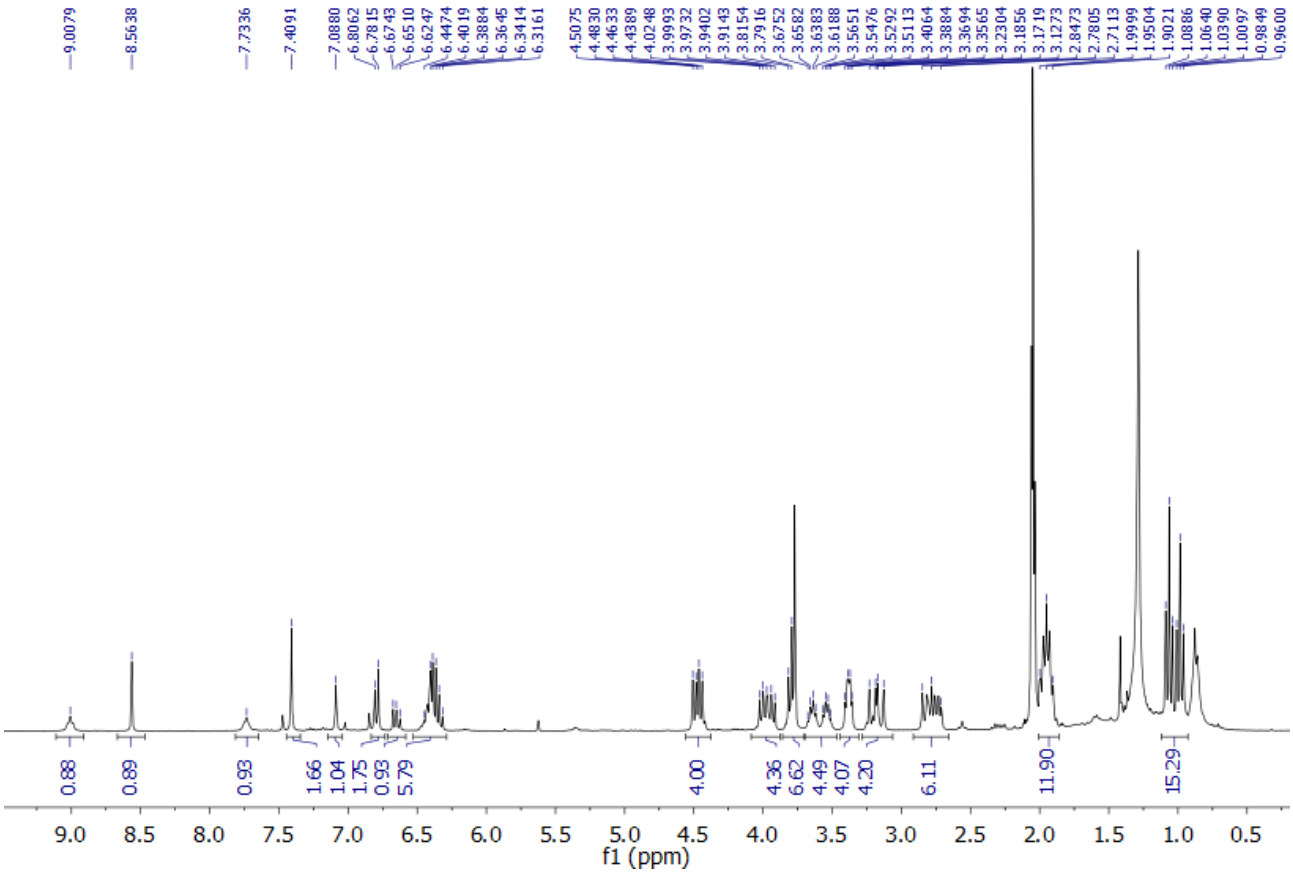

^{1}H NMR spectrum (acetone-d_6, 300 MHz) of compound **2**

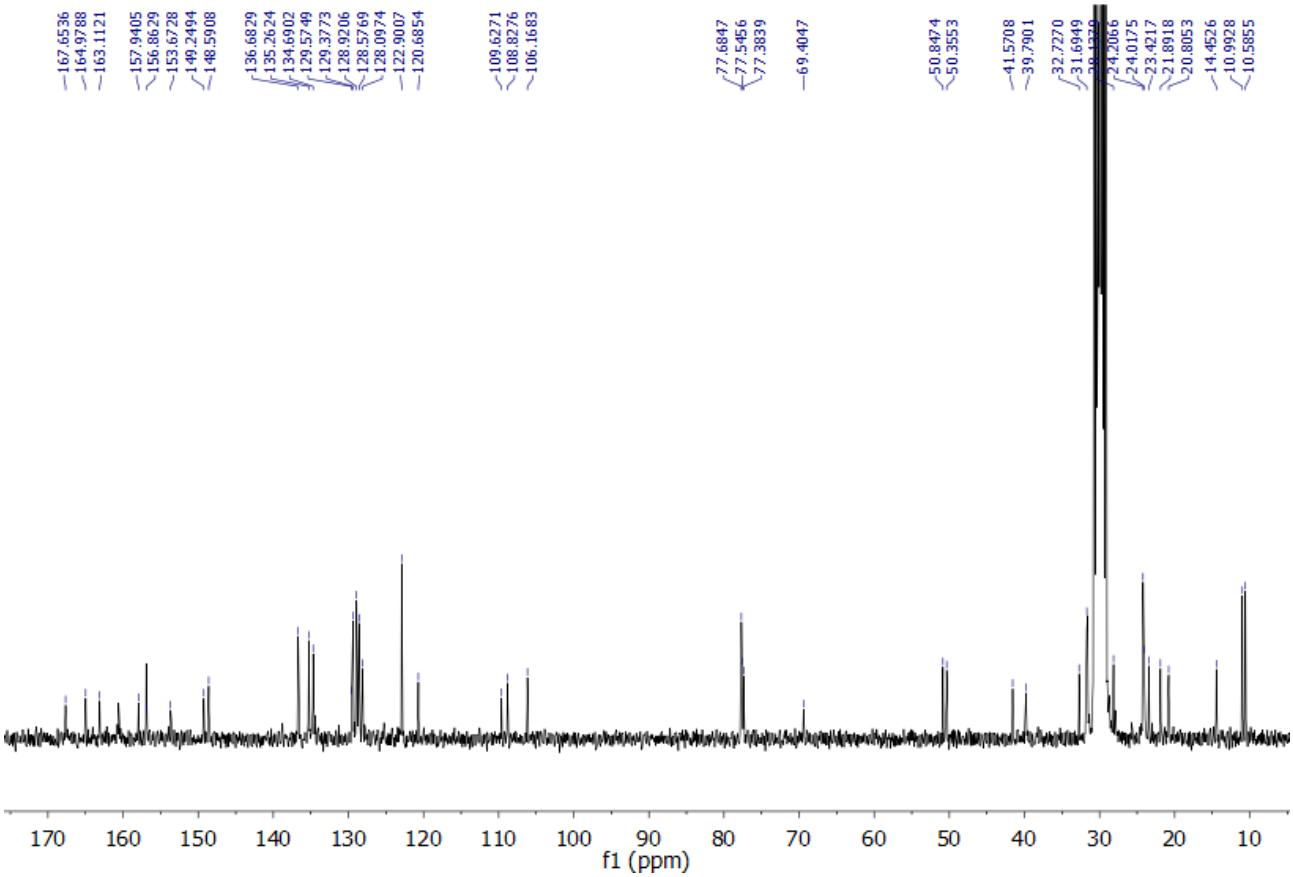

^{13}C NMR spectrum (acetone-d_6, 75 MHz) of compound **2**

4. CONFORMATIONAL PROPERTIES OF 25,26,27,28-TETRAPROPOXYCALIX[4]ARENES

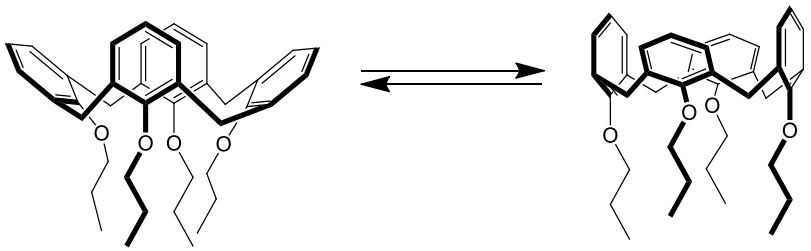

Figure S1. Fast interconversion of 25,26,27,28-tetrapropoxycalix[4]arene between two *flattened cone* conformations.

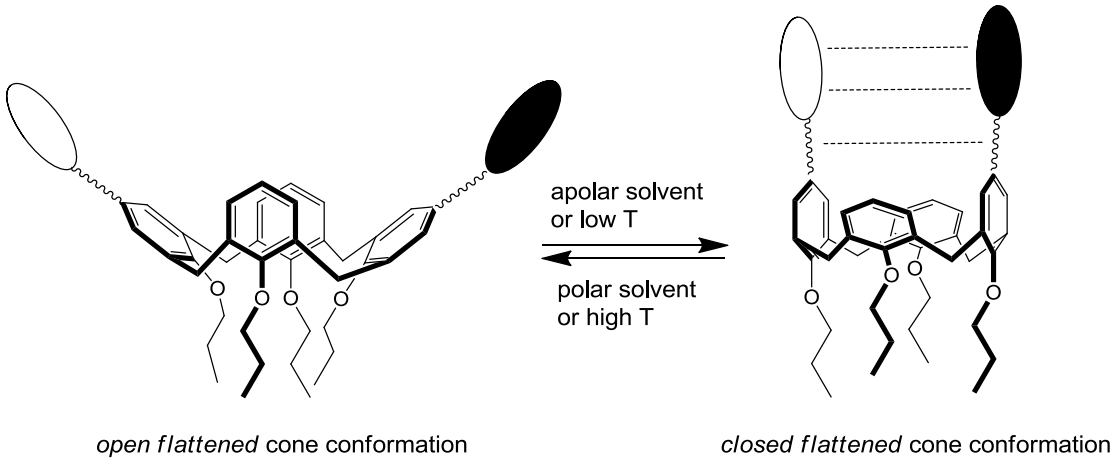

Figure S2. Schematic representation of the possible modulation of the interchromophore distance according to an external stimulus.

5. ^{1}H NMR STUDIES

Conformational analysis of compound 1 in different solvents

The ^{1}H NMR signals of the aromatic protons of the macrocycle are diagnostic of conformational changes and can be exploited to assess if a calix[4]arene difunctionalized on the distal positions of the upper rim adopts an "*open*" or "*closed*" *flattened* cone conformation (see Figure S2). In particular, the aromatic rings pointing outwards exert a shielding effect on the two aromatic rings that are parallel to each other and thus induce an upfield shift of their signals.

In Figure S3, the aromatic regions of the ^{1}H NMR spectra of **1** dissolved in DMSO-d_6 and in $CDCl_3$ are reported. The aromatic protons *ortho* to the upper rim substituents resonate at 7.59 and 7.57 ppm in DMSO-d_6, while their chemical shift is 6.70 and 6.53 ppm in $CDCl_3$. The signals of the non-substituted aromatic rings, on the contrary, are shifted downfield upon increase of the solvent polarity. These solvent-induced shift indicate that in DMSO-d_6 the calixarene adopts an "*open*" *flattened* cone conformation, while in $CDCl_3$ the calixarene is "*closed*".

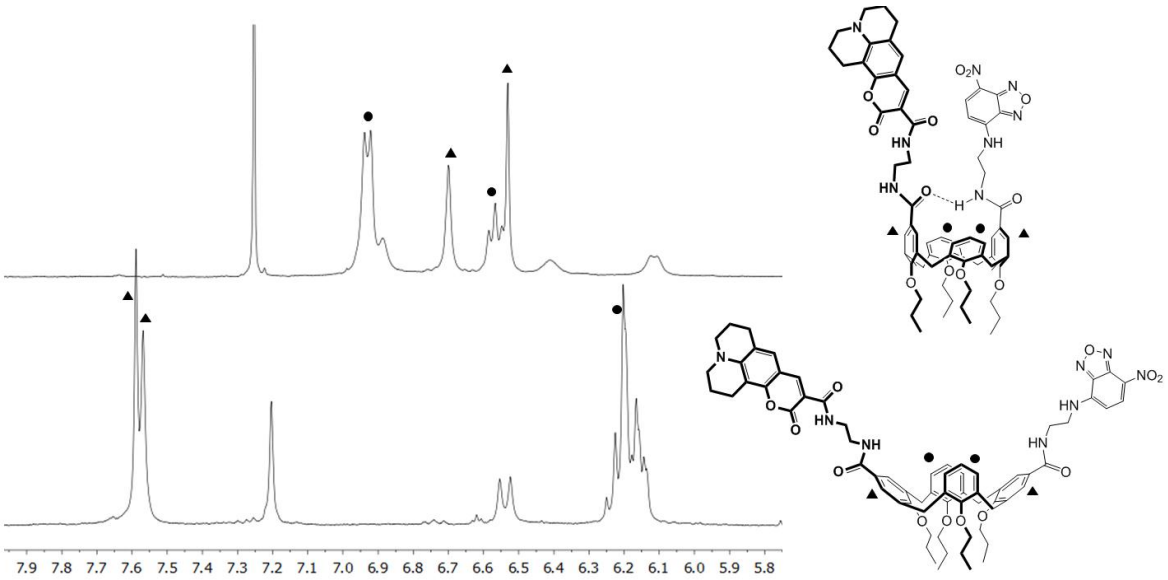

Figure S3. Left: portions of ^{1}H-NMR spectra of compound **1** in $CDCl_3$ (top) and DMSO-d_6 (bottom); right: schematic representation of the variation of conformation.

^{1}H NMR spectra of compound 1 at different concentrations

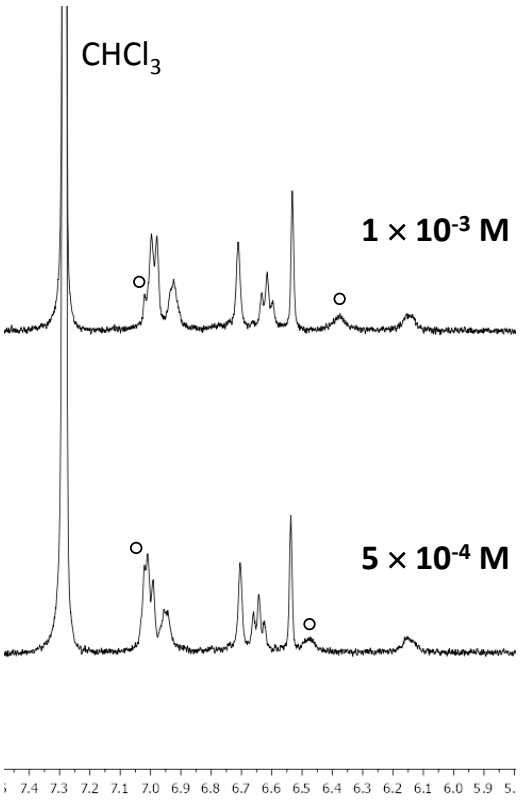

Figure S4. Portions of ^{1}H-NMR spectra (23°C) of compound **1** in $CDCl_3$ at different concentrations (top: 10^{-3} M, bottom: 5×10^{-4} M). The small shifts of the NH signals (circles) are due to the relative variation of water content in the solution.

Conformational analysis of compound 2 at different temperatures

In Figure S5, the aromatic regions of the ^{1}H NMR spectra of **2** in $CDCl_3$ at two different temperatures are reported, together with the plot of the chemical shifts of the aromatic protons of the substituted ring (triangles) and of the two unsubstituted rings in 1,3-position (circles). In the explored temperature range, when the solution is cooled down the signals of the substituted ring shift slightly downfield, while those of the unsubstituted rings move slightly upfield. Though quite small, these shifts are indicative of an "opening" of the calixarene scaffold at low temperature. The conformational behavior of reference compound **2** is therefore opposite to the behavior of compound **1**, which is characterized by a "closure" of the scaffold when the temperature is lowered. This is a confirmation that the conformational variation of compound **1** is due to the presence of intramolecular H-bonds.

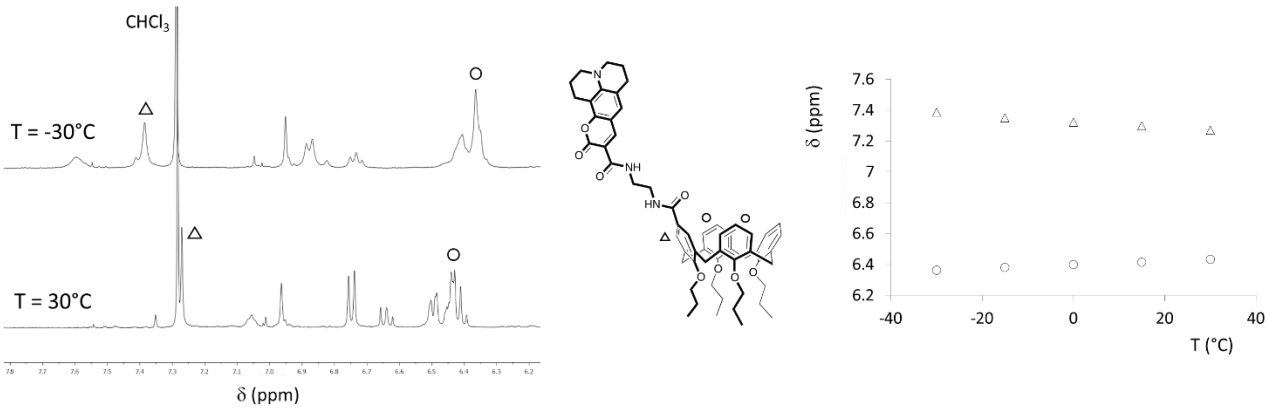

Figure S5. Left: portions of ^{1}H-NMR spectra of compound **2** in $CDCl_3$ at different temperatures; the symbols are referred to the molecular structure in the middle. Right: chemical shift of aromatic protons of **2** as a function of temperature.

6. SPECTROSCOPIC CHARACTERIZATION

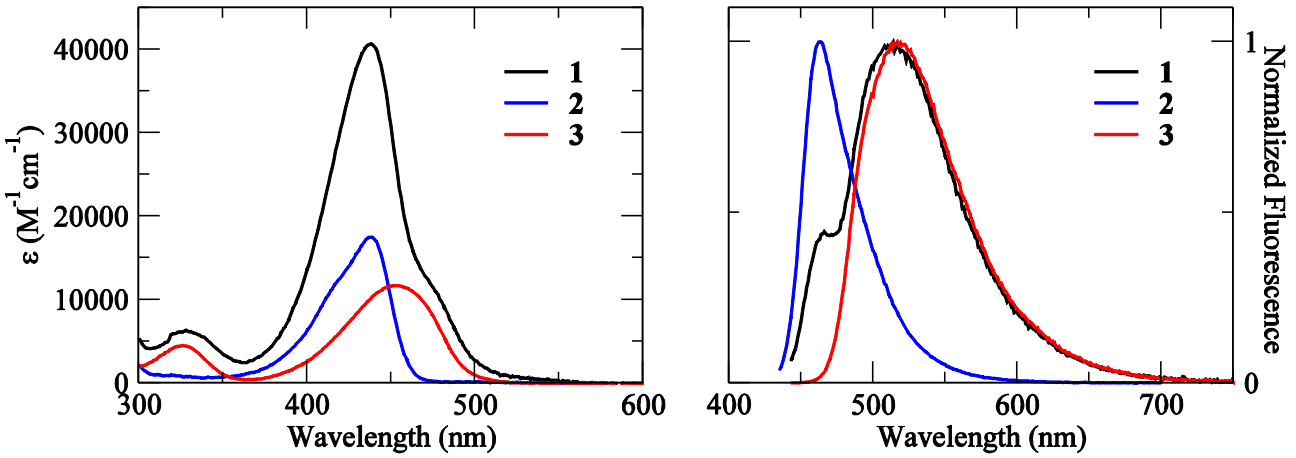

Figure S6. Molar extinction coefficient (left) and normalized emission intensity (right) of **1**, **2** and **3** in $CHCl_3$ at room temperature.

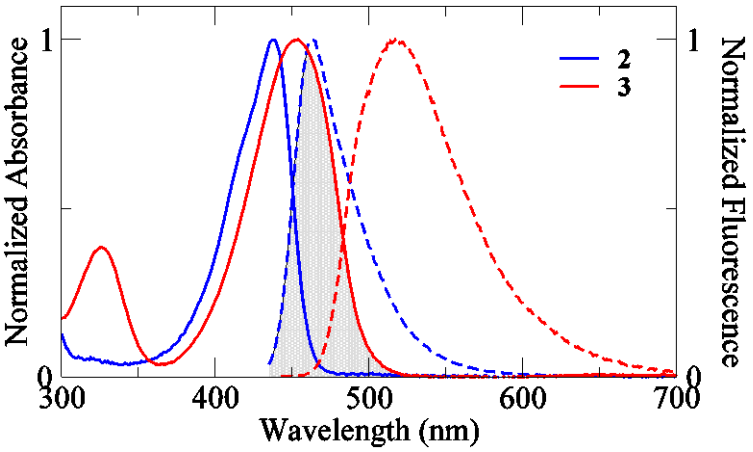

Figure S7. Absorption and fluorescence spectra of **2** and **3** in $CHCl_3$ at room temperature. The greyed area corresponds to the spectral overlap between the emission of **2** and the absorption of **3**.

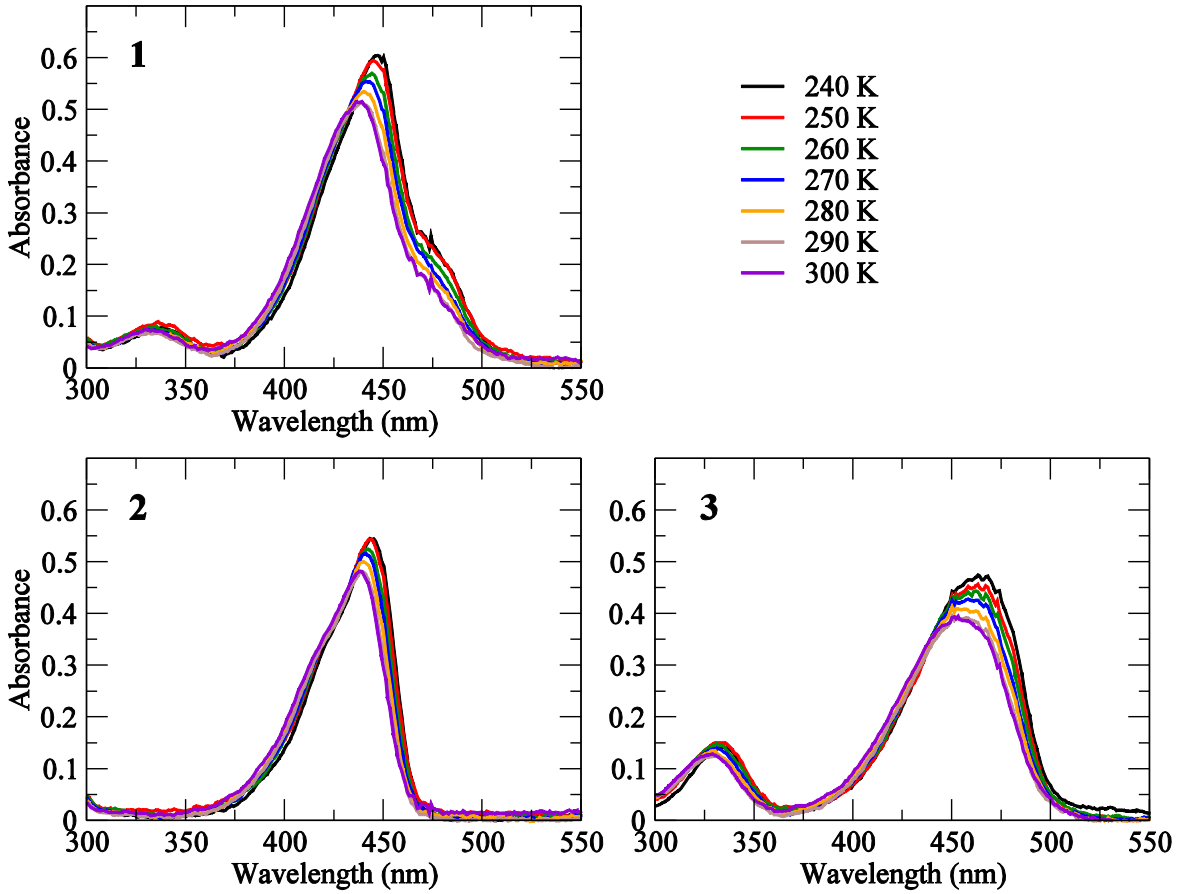

Figure S8. Absorption spectra of the bichromophore **1** and of the reference chromophores **2** and **3** measured in chloroform at different temperatures.

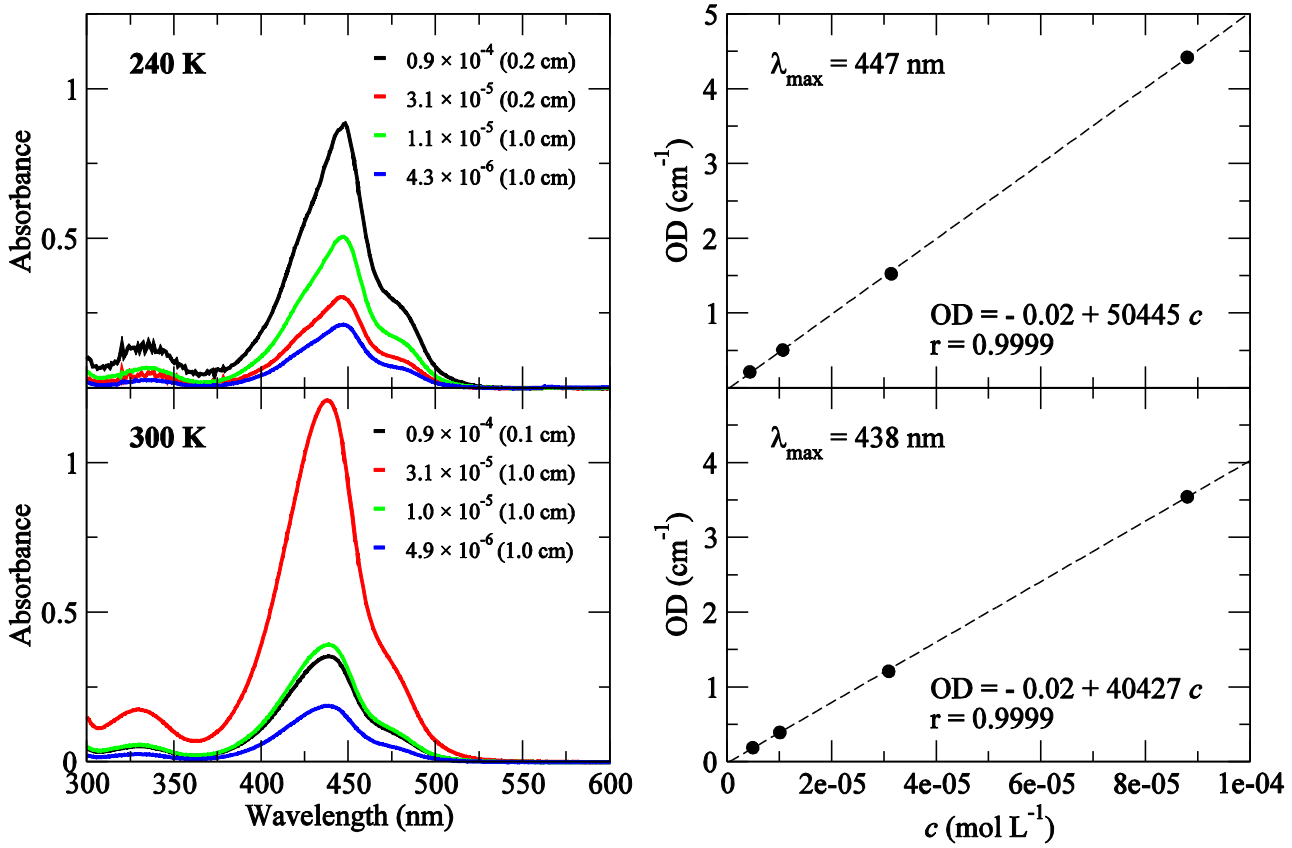

Figure S9. Verification of the Lambert-Beer law for compound **1** in $CHCl_3$ at the two limiting temperatures. Left panels: raw absorption spectra; Left panels: optical density (A/d) at the peak as a function of the concentration (dashed lines: linear regressions, with corresponding equations and linear correlation coefficients).

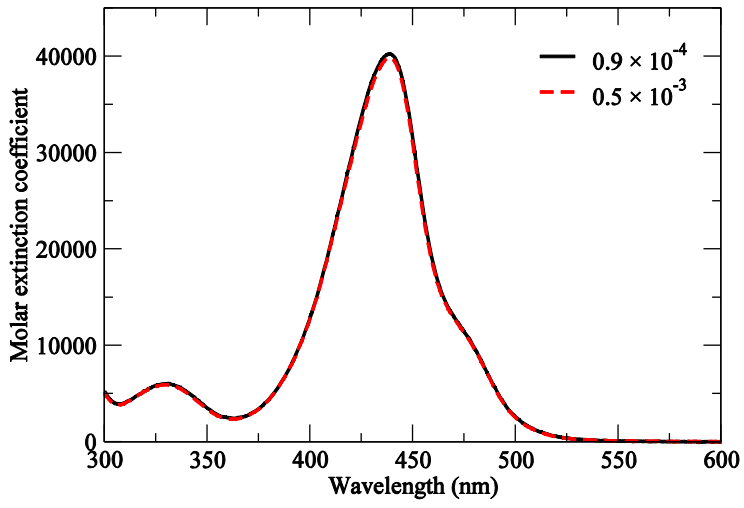

Figure S10. Comparison of the molar extinction coefficient spectrum of **1** obtained for a 10^{-4} M $CHCl_3$ solution and for a 0.5×10^{-3} M $CDCl_3$ solution (the same used for NMR spectra).

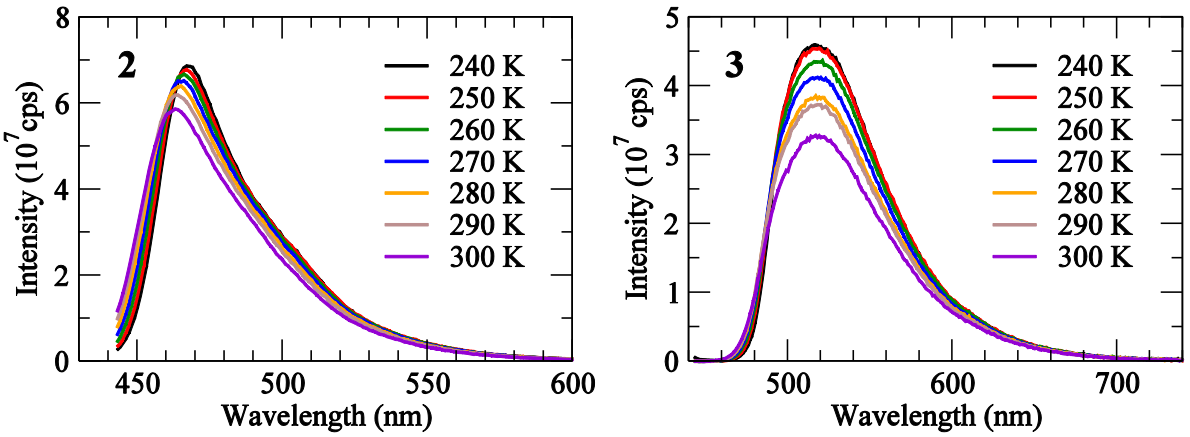

Figure S11. Fluorescence spectra of the reference compounds **2** and **3** in chloroform at different temperatures for excitation at 438 nm.

Table S1. Fluorescence quantum yields of reference compounds **2** and **3** at different temperatures (λ_{exc} = 438 nm; c = 3×10^{-6} mol L^{-1}). The uncertainty is estimated to amount to ~10%.

Temperature (K)	ϕ	
	2	**3**
240	1.00	0.73
250	0.97	0.73
260	0.99	0.68
270	0.97	0.65
280	0.98	0.61
290	1.00	0.62
300	0.94	0.53

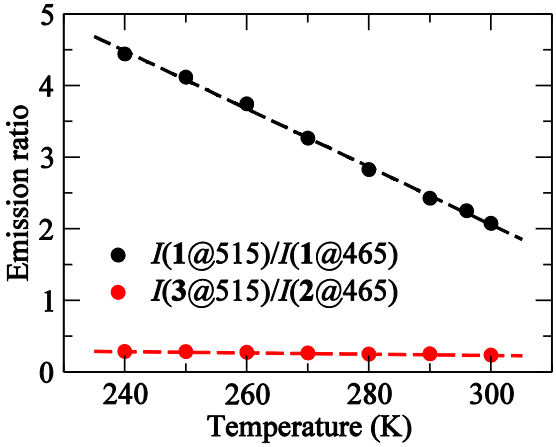

Figure S12. Black: ratio between the emission intensity of the bichromophore **1** at 515 nm and at 465 nm. Red: ratio between the emission of the reference acceptor **3** at 515 nm and the emission intensity of the reference donor **2** at 465 nm.

Evaluation of the FRET efficiency through the sensitization of the acceptor emission in 1 (method A)

Fluorescence Resonance Energy Transfer (FRET) occurs when the excited donor transfers (part of) its excitation energy to the energy acceptor. As a consequence of FRET, the fluorescence intensity of the energy donor decreases and, at the same time, the fluorescence intensity of the energy acceptor increases. The estimation of the variation of fluorescence intensity is not trivial. First of all, emission intensity can be strongly affected by several factors, and it is not guaranteed that energy transfer is the only phenomenon affecting the emission intensities of the energy donor and acceptor in the bichromophore (for example new non radiative decay paths could take place other than FRET). Moreover, when the absorption bands of the energy donor and of the energy acceptor are broad and strongly overlapped, it is not always possible to selectively excite one of the two chromophoric units (in this case the donor cannot be selectively excited).

In order to compare the emission intensity of the sole NBD chromophoric unit in **3** and in **1** in the absence of FRET, **1** was excited at 480 nm, where only NBD absorbs: the fluorescence quantum yield decreases from 0.62 in **3** to 0.23 in **1**. This result suggests the activation of new non-radiative decay paths in the bichromophore, independent of FRET (FRET from NBD to Coumarin343 can be ruled out because of the negligible overlap between the emission of NBD and the absorption of Coumarin343). In order to evaluate the efficiency of FRET from Coumarin343 to NBD in **1**, the emission intensity of NBD in **1**, obtained when NBD is selectively excited, has to be used as a reference.

To estimate the efficiency of FRET through the sensitization of the emission of the acceptor, we applied the following equation:

$$\phi_{FRET} = \left[\frac{I_{A(D)}}{I_A} - 1\right]\frac{\varepsilon_A(\lambda_D^{ex})}{\varepsilon_D(\lambda_D^{ex})} \qquad \text{(eq. S1)}$$

where $\varepsilon_{A/D}$ are the molar extinction coefficients of the reference chromophores **3** and **2** at the excitation wavelength λ_D^{ex} (in this case λ_D^{ex} = 438 nm); I_A is the emission intensity of the acceptor in **1** when FRET does not occur; $I_{A(D)}$ is the emission intensity of the acceptor in **1** when FRET occurs.

$I_{A(D)}$ has been estimated through deconvolution of the emission of **1** as the sum of the emission spectra of **2** and **3**. In order to obtain the correct emission intensity I_A to be used in eq. S1, we measured the emission intensity of **1** when selectively exciting NBD (i.e. at 480 nm), and rescaled for the absorbance at 480 nm vs the absorbance at 438 nm:

$$I_A(438nm) = \frac{I_A(480nm)\varepsilon(438nm)}{\varepsilon(480nm)}.$$

Evaluation of the FRET efficiency through the comparison between absorption and excitation spectra of 1 (method B)

The comparison between absorption spectra and excitation profiles of **1** obtained collecting emission from the sole acceptor (λ_{em} = 650 nm) is shown in Figure S13. This method requires that excitation spectra are normalized with respect to the absorption spectra as to have a correspondence of the spectral feature of the acceptor. The efficiency of the FRET process is estimated as the ratio between the excitation and absorption intensities in the region where only the donor absorbs. However, in our case, the absorption bands of **2** and **3** are largely overlapped, so that this procedure is not directly applicable. In particular, we have to carefully consider the contribution of the acceptor to the excitation spectrum. We performed a fitting of normalized absorption and excitation spectra of **1** as the sum of normalized absorption spectra of references **2** and **3** with suitable coefficients. The corresponding absorption and excitation spectra were then rescaled in order to get the same height of the acceptor contribution. From the comparison, and taking into account the contributions of the donor and of the acceptor, the efficiency of the FRET could be reliably estimated.

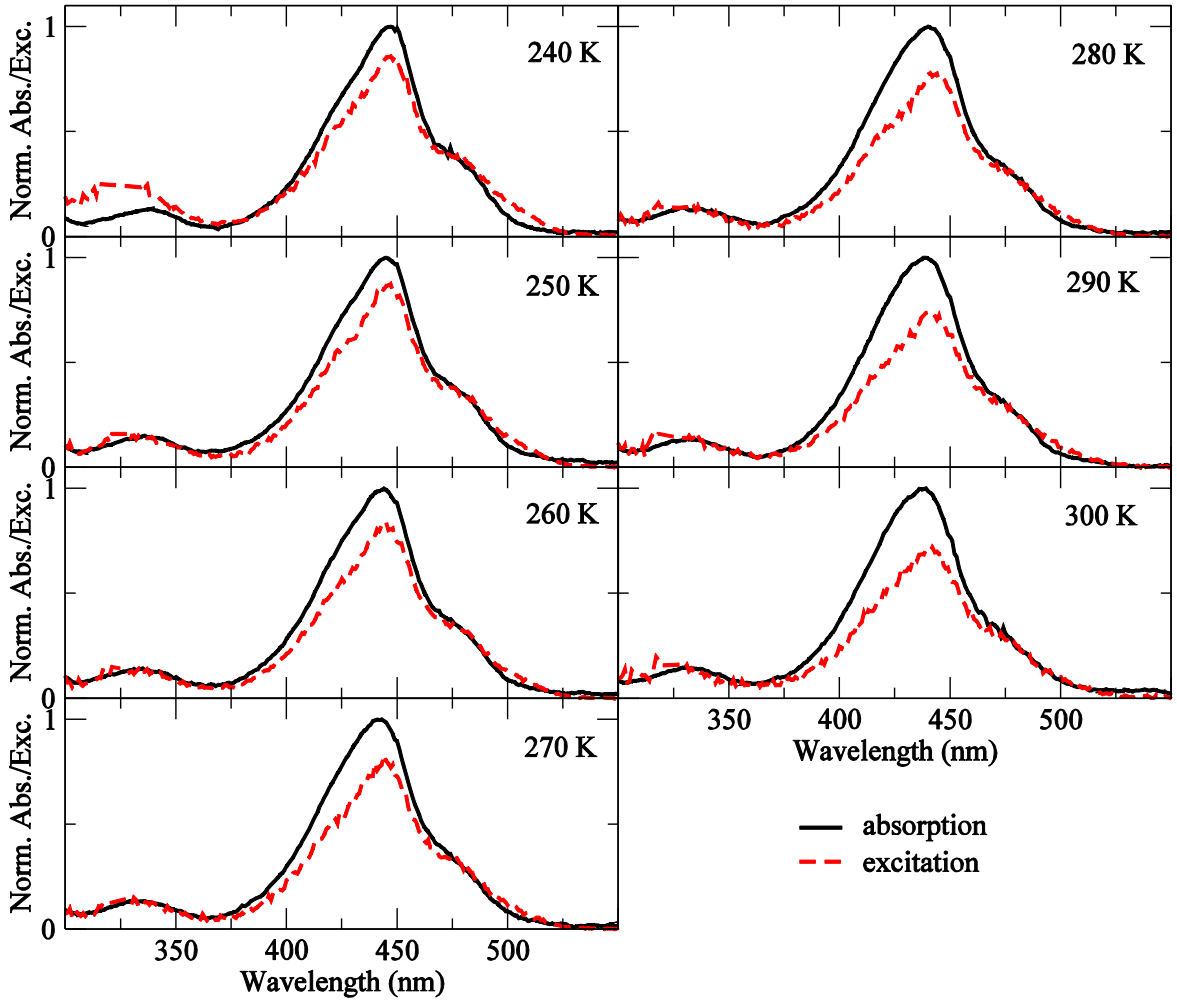

Figure S13. Comparison between absorption (black) and excitation (red) spectra of **1** collected for detection at 650 nm at different temperatures.

Temperature dependence of the refractive index

The refractive index of any solvent depends on temperature, typically increasing when the temperature is decreased. For chloroform, the refractive index varies from 1.4506 at 292 K to 1.4251 at 333 K.[5] Its thermal coefficient, $\mathrm{d}n/\mathrm{d}T$, is reported to amount to -6.5453×10^{-4}.[6] Using the measured value reported in Ref.[5] for the lowest temperature (292 K), we can extrapolate the refractive index of chloroform at the lower temperatures, as reported in Table S2.

Table S2. The refractive index of chloroform at different temperatures.[5,6]

Temperature (K)	n
240	1.4844
250	1.4779
260	1.4714
270	1.4648
280	1.4583
290	1.4517
300	1.4454

Effective Förster distance for the Coumarin343/NBD pair at different temperatures

The overlap integral between the emission of the donor and the absorption of the emission, entering eq. 1 of the main paper, is defined as:

$$J = \frac{\int I_D(\lambda)\varepsilon_A(\lambda)\lambda^4 d\lambda}{\int I_D(\lambda) d\lambda} \qquad \text{(eq. S2)}$$

where $I_D(\lambda)$ is the emission spectrum of the energy donor **2**, ε_A the molar extinction coefficient of the energy acceptor **3** (in units of $M^{-1}\,cm^{-1}$), and the integrals are performed on the wavelength scale over the range of the relevant bands.

Table S3. The overlap integral, J, and the effective Förster distances, R_k (incorporating the orientation factor), for the Coumarin343-NBD pair at different temperatures. Last column: effective interchromophore distance, r_k, in **1**, obtained based on the FRET efficiencies estimated through method B.

Temperature (K)	J (10^{14} $M^{-1}\,cm^{-1}\,nm^4$)	R_k (Å)	r_k (Å)
240	3.46	42.9	36.1
250	3.47	43.1	36.5
260	3.35	43.0	37.9
270	3.19	42.7	39.1
280	3.03	42.5	40.0
290	2.86	42.2	40.1
300	2.86	42.4	41.2

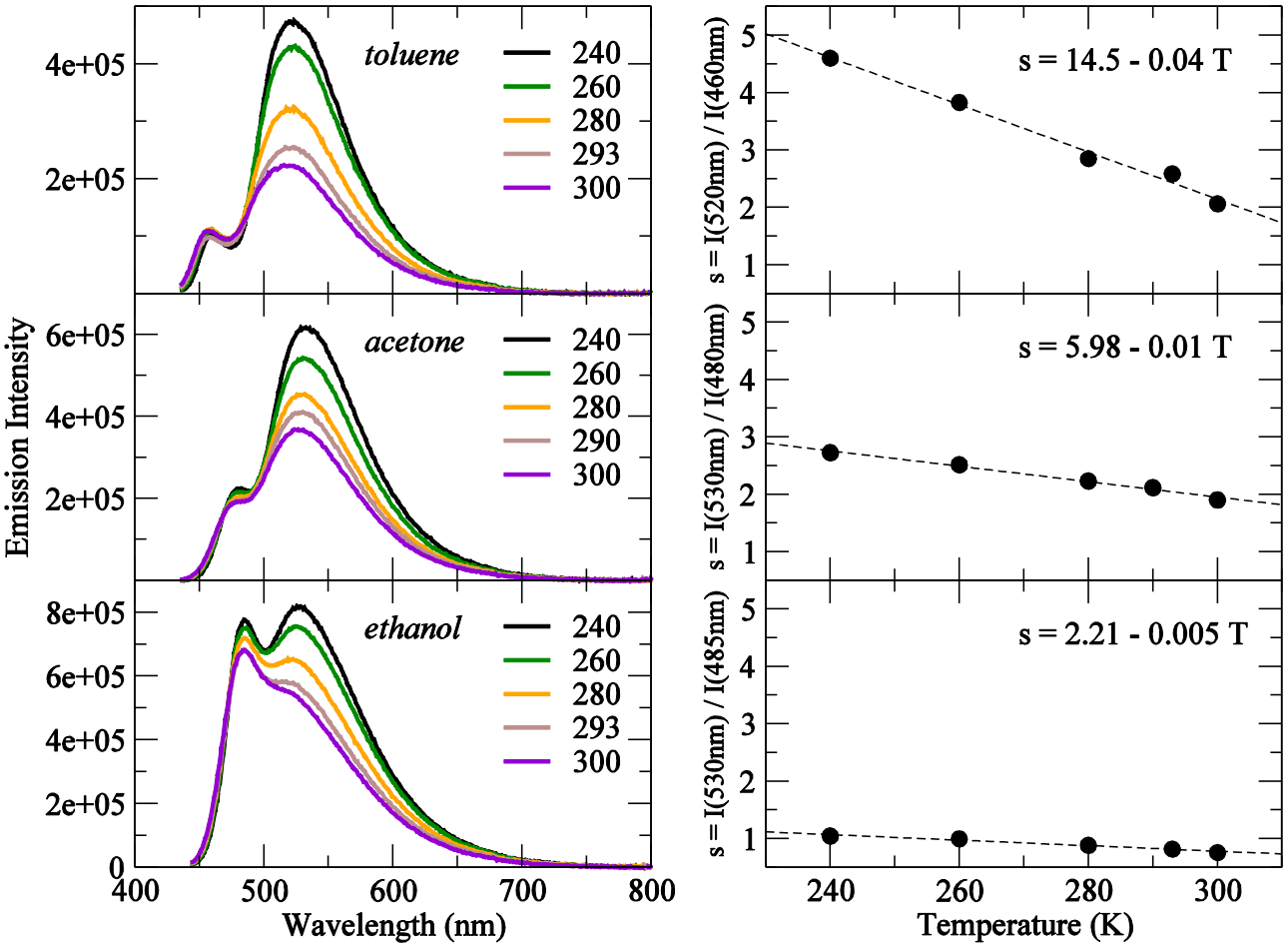

Figure S14. Left: emission spectrum of **1** in toluene, acetone and ethanol (from top to bottom) as a function of temperature (Kelvin). Right: temperature dependence of the ratio between the emission intensity of NBD and of Coumarin343 in **1** (dots: experimental data; dashed lines: linear fits), with corresponding equations in the legends.

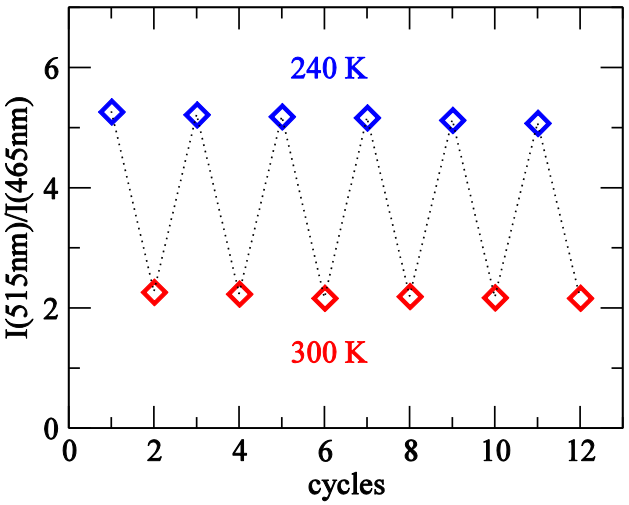

Figure S15. Reversibility/repeatability test of the ratiometric response of compound **1** over 12 cycles of cooling/heating of the same sample at 240 K (blue points) and 300 K (red points).

REFERENCES

1. F. Sansone, S. Barboso, A. Casnati, M. Fabbi, A. Pochini, F. Ugozzoli, and R. Ungaro, *Eur. J. Org. Chem.*, 1998, 897–905.
2. Z.-Y. Li, Y. Chen, C.-Q. Zheng, Y. Yin, L. Wang, and X.-Q. Sun, *Tetrahedron*, 2017, **73**, 78–85.
3. S. Taliani, F. Simorini, V. Sergianni, C. La Motta, F. Da Settimo, B. Cosimelli, E. Abignente, G. Greco, E. Novellino, L. Rossi, V. Gremigni, F. Spinetti, B. Chelli, and C. Martini, *J. Med. Chem.*, 2007, **50**, 404–407.
4. R. P. Briñas, T. Troxler, R. M. Hochstrasser, and S. A. Vinogradov, *J. Am. Chem. Soc.*, 2005, **127**, 11851–11862.
5. S. Valkai, J. Liszi, and I. Szalai, *J. Chem. Thermodyn.*, 1998, **30**, 825–832.
6. H. El-Kashef, *Rev. Sci. Instrum.*, 1998, **69**, 1243–1245.